# Self-adaptive photochromism

Fanxi Sun[1], Ang Gao[1], Boyun Yan[1], Jing Zhang[1], Xiangru Wang[1], Hanjun Zhang[1], Dacheng Dai[1], Yonghao Zheng[1]*, Xu Deng[2], Chen Wei[1]*, Dongsheng Wang[1]*

1. School of Optoelectronic Science and Engineering, University of Electronic Science and Technology of China, Chengdu 610054, China.
2. Institute of Fundamental and Frontier Science, University of Electronic Science and Technology of China, Chengdu 610054, China.

## Abstract

Camouflage is critically important because it improves the survival ability of animals when facing predators[1]. Some organisms (*e.g.,* chameleon, octopus) with an active camouflage ability exhibit a changeable appearance with switching of environments[2-4]. However, manmade active camouflage systems heavily rely on the integration of electronic devices, which encounters problems such as a complex structure, poor usability, and high cost[5-7]. In the current work, we report active camouflage as an intrinsic function of materials by proposing self-adaptive photochromism (SAP). The SAP materials were fabricated using donor-acceptor Stenhouse adducts (DASAs) as the negative photochromic phases and organic dyes as the fixed phases. Incident light with a specific wavelength induces *linear*-to-*cyclic* isomerization of DASAs, which generates an absorption gap at the wavelength and accordingly switches the color. The SAP materials are in the primary black state in the dark and spontaneously switch to another color upon triggering by transmitted and reflected light in the background. SAP films and coatings were fabricated by incorporating polycaprolactone and are applicable to a wide variety of surfaces. Our work reports SAP as a distinct intrinsic property of materials, guiding the development of source-free active camouflage and anticounterfeiting technology.

## Main

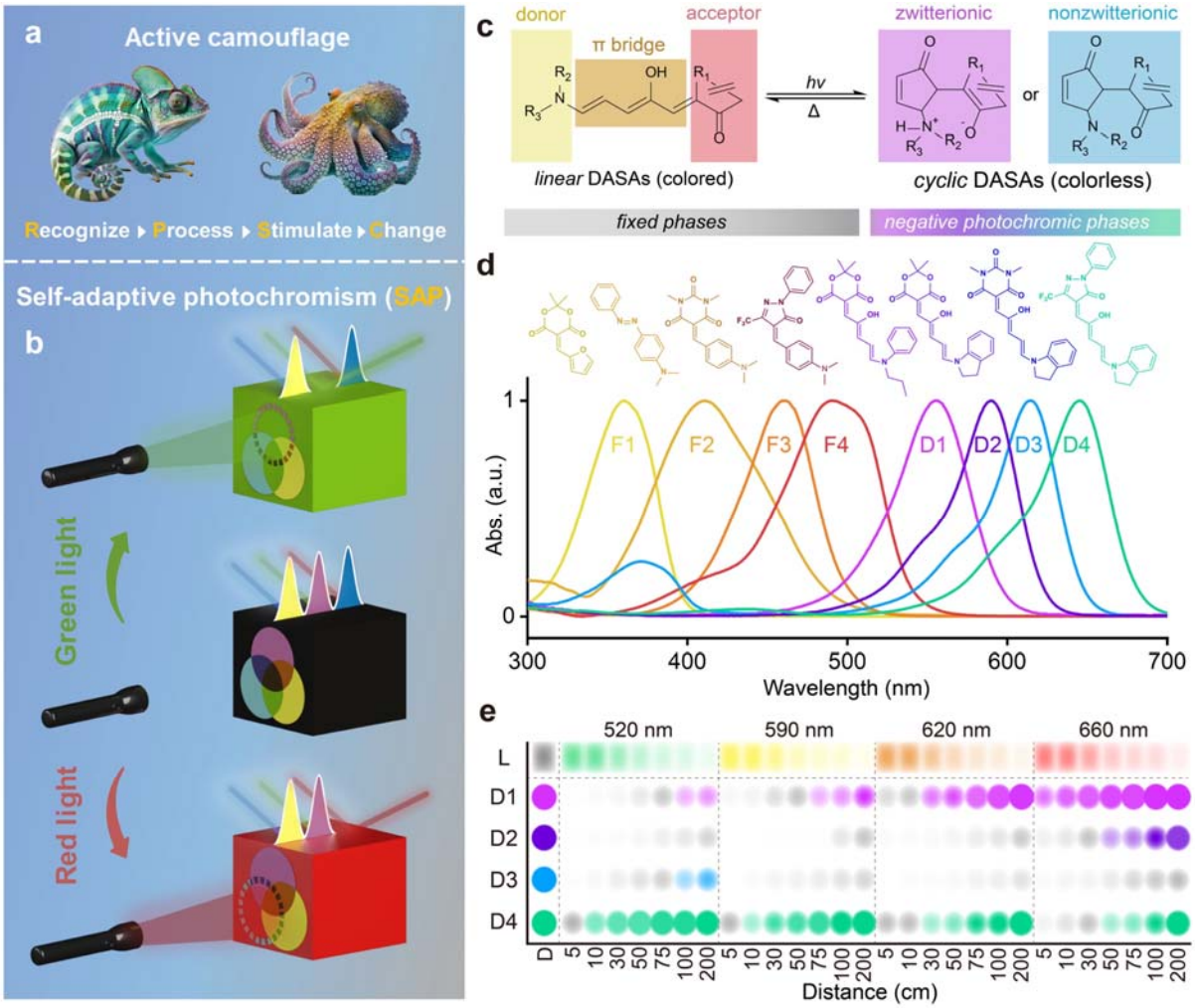


**Fig. 1 | Design of SAP materials. a**, Creatures with active camouflage (generated by Midjourney). **b**, Schematic illustration of the mechanism of SAP. **c**, General chemical structure and isomerization between *linear* and *cyclic* DASAs. **d**, Normalized UV–vis absorption spectra of the color-contributing units in fixed and negative photochromic phases (0.1 g/mL PCL in THF/DCM, 1:9 v/v). **e**, Relative color of DASAs under light irradiation with different wavelengths and distances.

Camouflage is a common and important trait of animals, including disruptive coloration[8] (Commerson's frogfish), self-decoration[9] (decorator crabs), mimesis[10] (flower mantis), distraction[11] (peacock butterfly), and active camouflage[2-4] (chameleon, octopus). Among them, active camouflage is attractive because the appearance could be altered to match the background, making the organisms difficult to recognize in different environments. This camouflage skill could be achieved by manmade systems through a sequential operation of recognize, process, stimulate, and change (**Fig. 1a**). The color of the environment is first recognized by a camera and then transformed into digital signals, which control stimuli

(*e.g.*, heat, electricity) to induce color switching of materials[5-7]. However, the systems heavily rely on the integration of electronic devices, which brings problems such as a complex structure, poor usability, and high cost.

One strategy is to make active camouflage an intrinsic function of materials. We propose self-adaptive photochromism (SAP), where the color of materials could be directly switched to and maintained the same as that of incident light. The design of SAP materials follows the theory of complementary colors[12]. The material exhibits an even absorption band in the entire visible light region, corresponding to black, in the dark (**Fig. 1b**). After exposure to light irradiation with a specific wavelength, the absorbance at this wavelength decreases, generating a gap in the absorption spectrum (**Fig. 1b**). This further switches the color of the SAP materials to match that of the incident light. To realize SAP, photoswitches (photochromic molecules) are needed that meet the following requirements: (1) exhibit a visible-light-induced colored-to-colorless transition (negative photochromism) and a thermal-dominated colorless-to-colored transition and (2) show a narrow and tunable absorption band in the visible light region.

Donor-acceptor Stenhouse adducts (DASAs) are selected as the photoswitches, which exhibit *linear*-to-*cyclic* isomerization under triggering by visible light, while the reverse *cyclic*-to-*linear* isomerization is thermally induced[13,14] (**Fig. 1c**). The *cyclic* isomer could be either zwitterionic or nonzwitterionic based on the chemical structure of electron-donating moieties[15-17]. The absorption spectra could be shifted by varying the electron-donating and electron-withdrawing moieties[15,18,19]. For the construction of SAP materials, DASAs termed D1[20] ($Abs_{max}$=556 nm), D2[15] ($Abs_{max}$=590 nm), D3[15] ($Abs_{max}$=614 nm), and D4[21] ($Abs_{max}$=645 nm) were synthesized and used as the negative photochromic phases (**Fig. 1d** and **Extended data Fig. 1**). Because of the push-pull nature of DASAs, blueshifting of the absorption spectra encounters obstacles and thus does not cover the entire visible light region[14]. Thus, organic dyes (F1-F4)[13,22] with absorption bands between ~300 nm and ~550 nm were used as the fixed phases (**Fig. 1d** and **Extended data Fig. 1**). Notably, the fixed phases do not show photochromism.

All the DASAs exhibit a sharply decreased absorption band in the visible light region with the *linear*-to-*cyclic* isomerization, which results in colored-to-colorless switching (**Extended data Fig. 2c-f**). The reverse *cyclic*-to-*linear* isomerization spontaneously occurs in the dark[23]. Typically, D4, as the third generation of DASAs, shows fast thermal relaxation, which induces an increase in the absorbance band during the scanning of spectra[18] (**Extended data Fig. 2f**). DASAs are in an equilibrium state (photostationary state) between *linear* and *cyclic* under light irradiation, and the *linear* content closely interrelated with the light conditions (*i.e.,* wavelength, intensity) determines the color of SAP materials. Light-emitting diodes (LEDs) with emission wavelengths of 520 nm (green), 590 nm (yellow), 620 nm (orange) and 660 nm (red) were selected to switch the color of the SAP materials. The dynamics of the photoisomerization of DASAs under LED triggering were investigated to determine the *linear* content at equilibrium. The intensity of the irradiation was adjusted by controlling the distance between the LEDs and samples, ranging between 5 and 200 cm (**Extended data Fig. 3a**). With increasing distance, the intensity of the light irradiation monotonically decreases (**Extended data Fig. 3b** and **Supplementary Table 1**).

DASA solutions in a mixture of tetrahydrofuran (THF), dichloromethane (DCM) and polycaprolactone (PCL) were used. The *linear*-to-*cyclic* isomerization of all the DASAs follows first-order kinetics, and the *linear* content at equilibrium ($L_e$) could be obtained by fitting through the following equation[15,24] (**Extended data Fig. 3b and Supplementary Table 4-32**).

$$L = L_e + L_1 \times e^{\left(-\frac{t}{t_0}\right)} \quad (1)$$

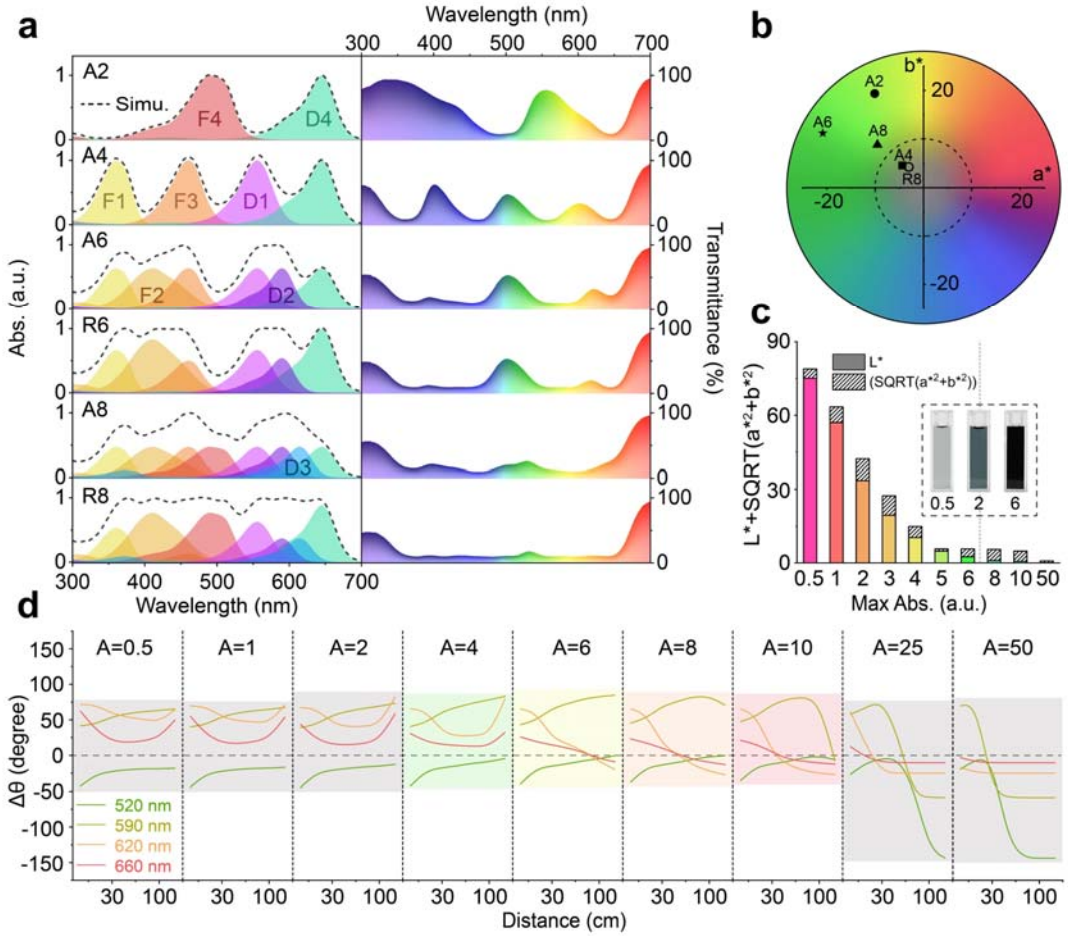


**Fig. 2 | Optimization of SAP materials. a**, Simulated UV–vis absorption (left) and transmission (right) spectra of SAP solutions with various combinations. **b**, Modified CIE 1931 *a* b** values of SAP solutions. **c**, Calculated lightness (*L*, colored solid*) and deviation (SQRT($a^{*2}+b^{*2}$), diagonal filled) values of the A4 solutions with initial absorbance between 0.5 and 50; the inset shows photographic images of A4 solutions with the initial absorbance of 0.5, 2 and 6. **d**, Accuracy of the color (Δθ) of A4 solutions under light irradiation with various conditions (wavelength and distance).

In the first-order kinetics, $L$ and $t_0$ represent the *linear* content (%) at irradiation time $t$ and the fitted time to reach equilibrium, respectively. The fitted *linear* content at equilibrium for the DASAs under light irradiation with various wavelengths and intensities is shown in **Extended data Fig. 3b** and **Supplementary Table 32**. To make the tendency visual, the data of the *linear* content were transformed into color information and are summarized in **Fig. 1e**. With decreasing distance between the LEDs and samples, the *linear* content exhibits a monotonic decrease for all the DASAs (**Extended data Fig. 3b**). This results in the colorless appearance of DASAs (**Fig. 1e**). The matching between the absorbance spectra of DASAs and emission spectra of LEDs is critically

100 important for the promotion of photoisomerization. When the DASAs are irradiated by green light
101 (distance≤75 cm), D1, D2 and D3 exhibit a *cyclic*-rich equilibrium state (*linear* content<10%); in
102 contrast, most of D4 is in the *linear* form (**Extended data Fig. 3b**). Redshifting of the light
103 increases the *linear* content of D1 and enriches the *cyclic* isomer of D4. However, D2 and D3 are
104 mostly in the colorless *cyclic* form (*linear* content<30%) under light irradiation between 520 and
105 660 nm (**Fig. 1e** and **Extended data Fig. 3b**). These results might be attributed to the
106 thermodynamically stable *cyclic* isomers of D2 and D3[15,24-26]. Therefore, D1 and D4 could be
107 tuned over a wide range of lightness of color by controlling the wavelength and intensity of light,
108 which contributes to the diversity of color for the SAP materials.

109 For the construction of SAP materials, the constituents of the negative photochromic phases
110 and fixed phases were optimized. The selection, ratio and concentration of the organic dyes (F1-
111 F4) and DASAs (D1-D4) were considered. We propose two general strategies to construct the SAP
112 materials: (1) A, short for average, represents that all the color-contributing units show the same
113 peak value of the absorbance spectra; (2) R, short for ratio, represents that the ratio between the
114 color-contributing units is controlled to keep the accumulated absorbance spectra as flat as possible.
115 The compositions of the SAP materials include A2 (F4+D4), A4 (F1+F3+D1+D4), A6 and R6
116 (F1+F2+F3+D1+D2+D4), A8 and R8.

117 The absorbance spectra of the SAP materials were obtained through the accumulation of each
118 color-contributing unit using the following equation[27] (**Fig. 2a**).

119 $$A = a\varepsilon_{F1} + b\varepsilon_{F2} + c\varepsilon_{F3} + d\varepsilon_{F4} + e\varepsilon_{D1} + f\varepsilon_{D2} + g\varepsilon_{D3} + h\varepsilon_{D4} \quad (2)$$

120 The factors (a, b, c…) represent the contents (μM) of color-contributing units, and $\varepsilon_X$ ($\mu M^{-1}$)
121 represents the molar absorption coefficient obtained through the standard curve method[28]

(**Supplementary Fig. 9** and **Supplementary Table 2**). The composition of each SAP material is shown in **Supplementary Table 33.** The cumulative absorbance spectra were transformed into transmittance through $T = 10^{-A}$ (**Fig. 2a**). With increasing number of color-contributing units, the SAP materials gradually exhibit even and quasi-full absorbance and transmittance bands in the visible light region.

A modified CIE 1931 color space[29] with $a^*$ $b^*$ coordinates was obtained through the transmittance spectra to quantitatively determine the color[30] (**Fig. 2b** and **Supplementary Table 34**). All the SAP materials show a greenish pristine color in the dark. R6 (-34.0, 8.3) is located outside the diagram due to the large absorption gap at approximately 460-520 nm (**Fig. 2a and 2b**). Among them, A4 (-4.4, 4.6) and R8 (-3.1, 4.3) are close to the center of the diagram, indicating that the pristine color of these composites is sufficiently black, meeting the design of SAP materials. Interestingly, quasi-full absorption of visible light is not essential to produce an accurate black color. A4 with a uniformly distributed absorption band exhibits high accuracy of black color as well as concise composition (**Fig. 2a**). Therefore, A4 was selected for the construction of SAP materials.

The concentration of the color-contributing units is closely interrelated with the lightness ($L^*$) of SAP materials. The initial absorbance of A4 was varied between 0.5 and 50 (**Extended data Fig. 4a**). With increasing initial absorbance, the portion of transmitted light gradually decreases, while the transmittance spectrum switches from a uniformly distributed band (such as for A4) to an even band (such as for R8) (**Extended data Fig. 4c**). When the initial absorbance is kept between 0.5 and 4, the transmission light at 350~650 nm dominates the spectra, which results in a greenish pristine color for A4 (**Extended data Fig. 4b** and **4c**, **Supplementary Table 35**). A further increase in the initial absorbance cuts off the transmission of green light, making A4

slightly reddish. The value of $L^* + SQRT(a^{*2} + b^{*2})$ was calculated to quantitatively determine the color accuracy, where $SQRT(a^{*2} + b^{*2})$ represents the color deviation[29] (**Fig. 2c**). A lower value of $L^* + SQRT(a^{*2} + b^{*2})$ indicates that the pristine state of SAP materials is blacker. For A4 with a relatively low initial absorbance (0.5-4), $L^*$ is the main factor affecting the color accuracy. An increase in the initial absorbance induces a monotonic and sharp decrease in $L^*$; additionally, the variation in $SQRT(a^{*2} + b^{*2})$ is related to the initial absorbance (**Fig. 2c**). With increasing initial absorbance, A4 gradually switches from light gray (A=0.5) to deep green (A=2) and black (A=6), which corresponds well to the results in **Fig. 2c** and **Extended data Fig. 4b**. Consequently, the initial absorbance needs to be greater than 4 to ensure an accurately black pristine state for the SAP materials.

The color accuracy of the SAP materials under light irradiation was simulated. A4 with an initial absorbance between 0.5 and 50 was considered. The wavelength of light irradiation was set at 520, 590, 620 and 660 nm, and the distance between the light and sample was kept at 5~200 cm to control the irradiation intensity. The simulation was based on the *linear* content of DASAs at equilibrium under light irradiation (**Fig. 1e** and **Extended data Fig. 3b**). The photoisomerization of DASAs has been reported to show a concentration dependence, where the *linear* content at equilibrium increases with increasing concentration[31,32]. Under the same light conditions, we found that the *linear* content did not obviously change for the DASA solutions with initial absorbances ranging 1-25 (**Supplementary Fig. 11**). The absorption and transmission spectra of A4 under light irradiation with different wavelengths and intensities were calculated by accumulating the spectra of color-contributing units in the photostationary state (**Supplementary Fig. 12-20**). In the modified CIE 1931 color space, the color of incident light was expressed as a straight line through the center and in a specific direction[29] (**Extended data Fig. 4d** and **4f**). Light irradiation shifts the

dot representing the color of SAP materials toward the corresponding line. However, for all wavelengths of light, with decreasing distance, the color of A4 gradually deviates and exhibits a tendency to switch to yellow. These results might be attributed to the photoisomerization of both D1 and D4 under strong LED light (**Fig. 1e** and **Extended data Fig. 3b**). A4 exhibits a tunable range of color, which first increases with increasing initial absorbance of the solution. After reaching the maximum at A=6, the tunable range sharply decreases (**Extended data Fig. 4d-f**).

To quantitatively determine the color accuracy, the absolute difference in the angle between the dot and line ($\Delta\theta$) in the chromaticity diagram was calculated (**Extended data Fig. 4d** and **4f**). The results are summarized in **Fig. 2d** and **Supplementary Table 47-55**. When irradiated with green light, the color of A4 gradually approaches that of the incident light with increasing distance (**Fig. 2d**). For the A4 solutions with an initial absorbance between 4 and 10, $\Delta\theta$ reaches 0 at distances greater than 100 cm, indicating that the color deviation could be eliminated. Meanwhile, A4 with an initial absorbance of 6-10 exhibits accurate orange and red colors under 620 and 660 nm light irradiation, respectively. Therefore, for the construction of SAP materials, accounting for the color accuracy, A4 with an initial absorbance of 6 was selected.

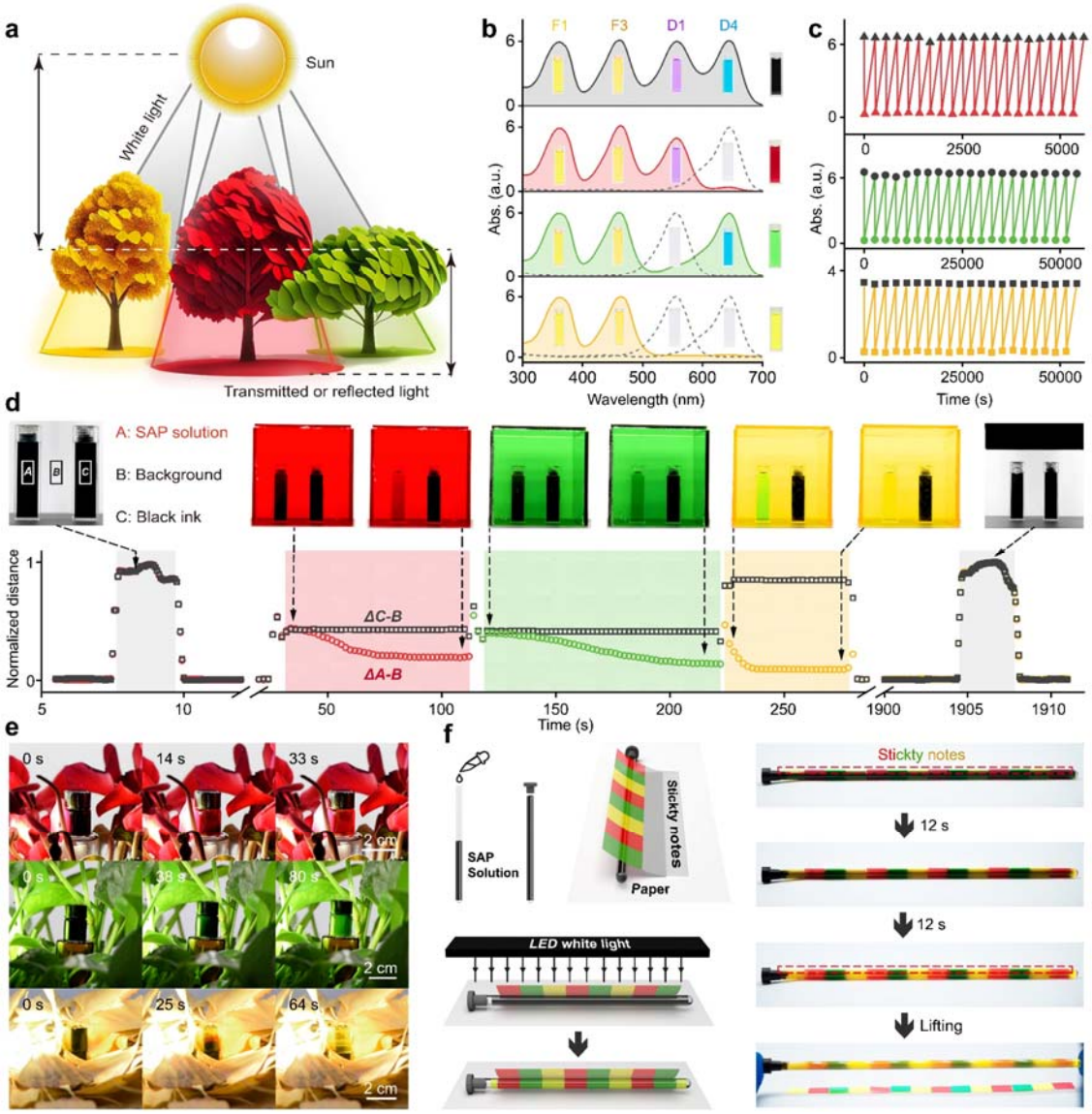


**Fig. 3 | SAP and active camouflage in solutions. a**, Schematic illustration of the philosophy for the active camouflage: the color of the environment depends on the transmitted and reflected light. **b**, Normalized UV-vis absorption spectra of the SAP solutions in the dark and under 660 nm, 520 nm, and 590 nm light irradiation, insert shows the photographic images of each color-contributing unit and the resulted SAP solutions (the spectra of 590 and 660 nm irradiation were obtained under the liquid nitrogen treatment). **c**, Fatigue resistance of SAP solutions switching of black-red (red line, absorbance at 644 nm monitored), black-green (green line, absorbance at 556 nm monitored), and black-yellow (yellow line, absorbance at 602 nm monitored) for 20 cycles. **d**, Color switching of SAP solutions in black, red, green and yellow acrylic boxes; the left cuvette was loaded with SAP solutions and the right cuvette with black ink as the control. Black dots represent the in situ distance between the average RGB values of regions C and B, and colored dots represent the distance between regions A and B. **e**, Video screenshots of the active camouflage of SAP solutions in red, green, and yellow bushes. **f**, Schematic illustration and video screen shots of realizing active camouflage by SAP solutions in an NMR tube covered by sequentially arranged sticky notes.

The achievement of active camouflage through SAP materials is based on the transmitted and reflected light of the background, which shows a specific wavelength according to the color of the

environment[33] (**Fig. 3a**). For example, when the SAP materials are placed in a green environment, the green transmitted and reflected light switches the SAP materials to green, which could thus be hidden in the background.

The photochromism of SAP solutions was investigated. Before light irradiation, the SAP solutions show a black pristine state, which switches to red, green and yellow under 660, 520 and 590 nm light irradiation (5 mW/cm$^2$) (**Fig. 3b**). Green light and red light generate gaps in the absorption spectra of the SAP solutions at 500-600 nm and 600-700 nm due to the *linear*-to-*cyclic* isomerization of D1 and D4, respectively. In contrast, 590 nm yellow light switches both D1 and D4 to the colorless *cyclic* state, and the resulting SAP solutions show the overlaid color of F1 and F3. The color switching of SAP materials between black, red, green and yellow is reversible (**Fig. 3c**). No obvious loss of absorbance[15] (645 nm for red, 556 nm for green, 602 nm for yellow) was noticed, indicating that the SAP materials are stable under light irradiation.

The active camouflage of SAP materials was evaluated by setting them in environments with different background colors. Cubic boxes of black, red, green and yellow were fabricated from acrylic boards. The transmission spectra of the boxes were recorded to determine the incident light information (**Extended data Fig. 5a**). Two cuvettes filled with the SAP solution (left) and nonswitchable black ink as the control (right) were placed in the boxes, and a white light LED (10000 lux) was used as the light source for triggering of photochromism as well as illumination. Both solutions were in the pristine state in the black box after 30 s (**Fig. 3d** and **Supplementary Video 1**). Placing the cuvettes in the red box switched the SAP solution to red in 80 s, which became difficult to identify by the naked eye. The SAP solution changed to green and yellow in 110 and 50 s in the green and yellow boxes. After being set in the black box, the SAP solution switched back to the pristine state. In contrast, the black ink remained black throughout the whole

process. Moreover, the acrylic boards could be used as filters set between the light and SAP materials, which accordingly switched the solutions to green, yellow, orange and red (**Extended data Fig. 5b** and **Supplementary Video 2**). We used self-written color-analysis software to quantitatively evaluate the performance of active camouflage of the SAP materials[34,35] (the source code is available in **Supplementary Information section 9**). The average RGB values in the fixed areas A (SAP solution), B (background) and C (black ink) were collected, and the absolute differences of A-B and C-B (ΔA-B and ΔC-B) were calculated, as shown in **Fig. 3d**. The SAP solution exhibited a monotonically decreasing ΔA-B value with time in the red, green and yellow boxes, indicating that the color gradually switched to the same color as the background. Therefore, the SAP materials could be hidden in the environment and exhibit active camouflage. In contrast, the ΔC-B value of the black ink did not change in any environment.

For real applications, the SAP materials were placed in red (*Cyclamen persicum*), green (*Epipremnum aureum*) and yellow (*Ginkgo*) bushes, and a white light LED was set to the left of the plants. The transmitted and reflected light in the bushes induced photochromism of the SAP materials, as shown in **Fig. 3a** and **Extended data Fig. 5d**. The reflectance spectra of the leaves were recorded, as shown in **Extended data Fig. 5c**, which well matched the absorbance spectra of the SAP materials. Taking *Cyclamen persicum* as an example, the leaves mainly reflect light above 600 nm, resulting in red incident light for the SAP materials. The SAP solutions gradually switched from black to red, green and yellow in the bushes of *Cyclamen persicum*, *Epipremnum aureum* and *Ginkgo*, respectively (**Fig. 3e** and **Supplementary Video 3** and **4**). An outdoor experiment was conducted under sunlight (60000 lux, 37 °C, and bottles were stored in the dark and immersed

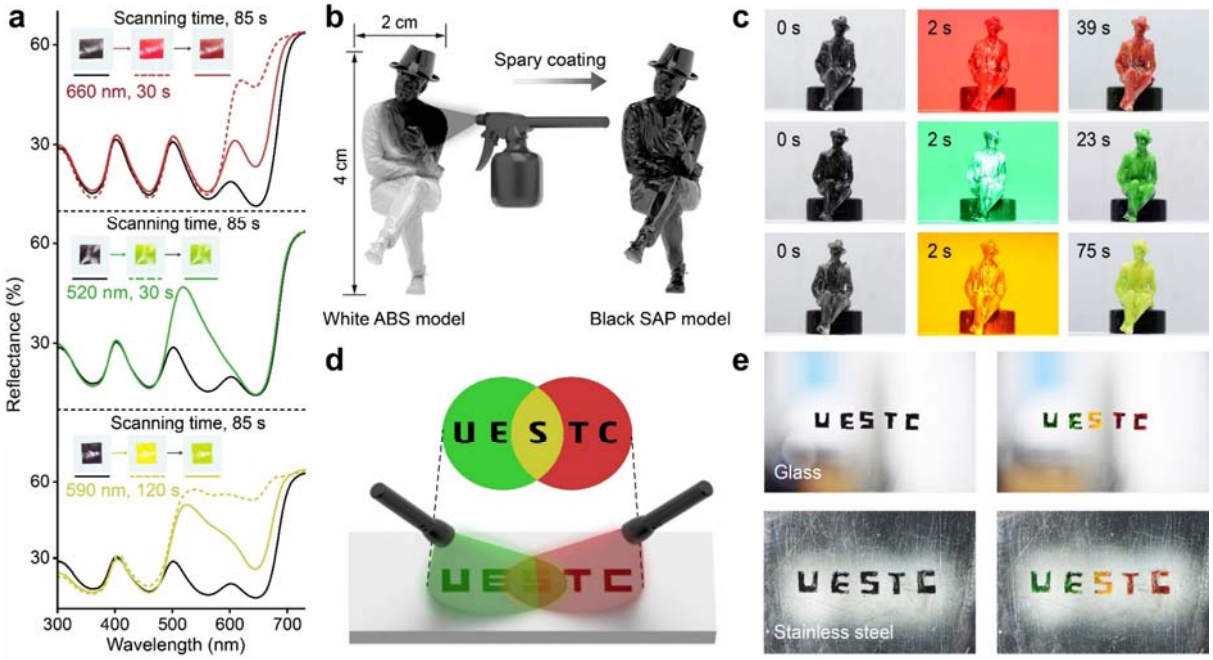


**Fig. 4 |SAP in films and coatings. a**, UV–vis diffuse reflectance spectra of SAP films before (black, solid) and after (colored) 660 nm (95 mW/cm$^2$, 30 s), 520 nm (140 mW/cm$^2$, 30 s), and 590 nm (25 mW/cm$^2$, 120 s) light irradiation; the spectra were recorded under room temperature (solid) and liquid nitrogen (dashed), and the inserts show photographic images of the SAP films before irradiation, immediately after irradiation, and after 85 s scanning. **b**, Schematic illustration of spray coating an SAP solution on the surface of a white ABS model. **c**, Video screenshots of the SAP process of three black ABS models in response to 660 nm (top), 520 nm (middle) and 590 nm (bottom) light. **d**, Schematic illustration of irradiating the "UESTC" by green and red light. **e**, Photographic images of SAP coatings on smooth surfaces (glass and stainless steel) before (left) and after (right) light irradiation.

in liquid nitrogen for 5 s before the experiments), in which umbrellas of green, yellow, orange and red were used (**Extended data Fig. 6**). The SAP solutions accordingly switched and could be hidden under the umbrella (**Extended data Fig. 6** and **Supplementary Video 5** and **6**).

The addition of PCL increases the viscosity of SAP solutions, which slows the diffusion of color-contributing units. Therefore, we expect that semisolid SAP materials could mimic surrounding patterns with different colors, similar to octopuses. The SAP solution was filled into a nuclear magnetic resonance tube, which was covered with sequentially arranged red, green and yellow sticky notes (**Fig. 3f**). A white light LED was set on the top. With irradiation, the SAP solution gradually switched from black to polychromic, making the sticky notes difficult to recognize (**Fig. 3f** and **Supplementary Video 7**). The SAP solution exhibited a periodic yellow-red-green arrangement, which well-matched the color of the above sticky notes.

Photochromism in the solid state furthers the applications of SAP materials in the real world.[36] PCL with a low glass transition temperature (-60 °C) and rich ester functional groups is an important matrix to efficiently promote the isomerization between *linear* and *cyclic* DASAs. On the one hand, the rubbery state of PCL at room temperature provides sufficient free space for molecular isomerization; on the other hand, the rich ester groups thermodynamically promote the *linear*-to-*cyclic* isomerization of DASAs by facilitating the process of intermolecular proton transfer[37].

The SAP solution was spin-coated onto the surface of a glass substrate, and after gentle peeling off, an SAP film was fabricated. The SAP film was in the black pristine state and switched to red, green and yellow after 660, 520 and 590 nm light irradiation (60 mW/cm$^2$), respectively (**Fig. 4a** and **Supplementary Video 8**). Compared to the solution, the SAP film needs a higher intensity of light and a longer irradiation time for photochromism, which is attributed to the hindered photoisomerization of DASAs in the solid state[36]. The reflectance spectra of the SAP film after light irradiation are recorded in **Fig. 4a**. Due to the fast thermally induced *cyclic*-to-*linear* isomerization of D4, the reflectance spectra of the SAP film after 660 and 590 nm light irradiation were difficult to capture[18]. More than 50% of *cyclic* D4 relaxed to the *linear* form during the scanning process (85 s), resulting in color deviation (solid line in **Fig. 4a**). Liquid nitrogen was used immediately after light irradiation to obtain the reflectance spectra of the SAP film (dashed line in **Fig. 4a**).

Coating is an attractive and important application for SAP materials. The SAP solution was spray coated onto the surface of a figurine model made of acrylonitrile butadiene styrene (ABS) plastic (**Fig. 4b**). A rapid annealing process generated a homogenously black and smooth surface of the figurine (**Supplementary Fig. 22-23**). Light irradiation at 660, 520 and 590 nm (60 mW/cm$^2$)

was used to trigger photochromism of the SAP coating. The figurine switched to red, green and yellow after light irradiation for 20~80 s (**Fig. 4c** and **Supplementary Video 9**). Notably, the irradiation time for photochromism of the SAP coating is similar to that for the SAP film, where the 590 nm yellow light takes the longest time (**Fig. 4a** and **4c**) because the yellow light is located between the absorbance spectra of D1 and D4. The word "UESTC" (abbreviation for the University of Electronic Science and Technology of China) was recorded by spray coating the SAP solution through a mask (**Fig. 4d** and **Extended data Fig. 7a**). Green and red LEDs were set separately on two sides of the substrate. The "UE" and "TC" were irradiated by green and red light, respectively. The "S" was simultaneously treated by green and red light, which resulted in yellow incident light. The SAP coating adapts well to a variety of surfaces, including glass, stainless steel, painted walls, A4 paper, wood and clothes (**Fig. 4e** and **Extended data Fig. 7b**). The black "UESTC" switched to polychromic after light irradiation, with green "UE", yellow "S" and red "TC". These results indicate that the SAP materials work well in the solid state.

In summary, we reported SAP of materials, where the color could be controllably switched to and maintained the same as that of incident light. DASAs (D1-D4) and nonphotochromic organic dyes (F1-F4) were used as the negative photochromic and fixed phases for the construction of SAP materials. Based on optimizing the selection, ratio and concentration of the color-contributing units, A4 constituted by F1, F3, D1 and D4 was chosen for the construction of SAP materials, where the initial absorbance was kept at 6. In the solution state, the SAP materials switched to green, yellow and red under 520, 590 and 660 nm light irradiation. More importantly, active camouflage was successfully achieved. In the environments with the background color of green (green acrylic box and umbrella, *Epipremnum aureum*), yellow (yellow acrylic box and umbrella, *Ginkgo*), orange (orange acrylic box and umbrella) and red (red acrylic box and umbrella,

*Cyclamen persicum*), the SAP materials switched accordingly. Active camouflage works well in polychromic backgrounds with complex patterns. By applying PCL as the matrix, films and coatings were fabricated to demonstrate SAP in the solid state.

SAP materials show great potential to be applied in camouflage systems, smart coatings, and display devices. However, there are still some challenges that must be addressed. Due to the limitation of the chemical structure of DASAs, the absorbance spectra of SAP materials could be controlled above 520 nm[14]. Therefore, purple and blue colors are missing for the current SAP materials. Future work could focus on developing negative photochromic molecules with an absorbance band in the blue light region. Overall, this work reported SAP as a distinct intrinsic property of materials, guiding the development of source-free camouflage and anticounterfeiting technology.

## References


1 Stevens, M. & Ruxton, G. D. The key role of behaviour in animal camouflage. *Biol. Rev.* **94**, 116-134 (2019).

2 Teyssier, J., Saenko, S. V., Van Der Marel, D. & Milinkovitch, M. C. Photonic crystals cause active colour change in chameleons. *Nat. Commun.* **6**, 6368 (2015).

3 Mäthger, L. M., Denton, E. J., Marshall, N. J. & Hanlon, R. T. Mechanisms and behavioural functions of structural coloration in cephalopods. *J. R. Soc. Interface* **6**, S149-S163 (2009).

4 Cuthill, I. C. *et al.* The biology of color. *Science* **357**, eaan0221 (2017).

5 Chou, H. H. *et al.* A chameleon-inspired stretchable electronic skin with interactive colour changing controlled by tactile sensing. *Nat. Commun.* **6**, 8011 (2015).

6 Kim, H. *et al.* Biomimetic chameleon soft robot with artificial crypsis and disruptive coloration skin. *Nat. Commun.* **12**, 4658 (2021).

7 Zhang, P. *et al.* Integrated 3D printing of flexible electroluminescent devices and soft robots. *Nat. Commun.* **13**, 4775 (2022).

8 Pietsch, T. W. & Grobecker, D. B. Frogfishes. *Sci. Am.* **262**, 96-103 (1990).

9 Hultgren, K., Stachowicz, J., Stevens, M. & Merilaita, S. Camouflage in decorator crabs: integrating ecological, behavioural and evolutionary approaches. *Animal camouflage*, 214-229 (2011).

10 Mizuno, T., Yamaguchi, S., Yamamoto, I., Yamaoka, R. & Akino, T. "Double-Trick" visual and chemical mimicry by the juvenile orchid mantis Hymenopus coronatus used in predation of the oriental honeybee Apis cerana. *Zool. Sci.* **31**, 795-801 (2014).

11 Vallin, A., Jakobsson, S., Lind, J. & Wiklund, C. Prey survival by predator intimidation: an experimental study of peacock butterfly defence against blue tits. *Proc. R. Soc. B* **272**, 1203-1207 (2005).

12 Algar, W. R., De Jong, C. A., Maxwell, E. J. & Atkins, C. G. Demonstration of the spectrophotometric complementary color wheel using LEDs and indicator dyes. *J. Chem. Educ.* **93**, 162-165 (2016).

13 Helmy, S. *et al.* Photoswitching using visible light: a new class of organic photochromic molecules. *J. Am. Chem. Soc.* **136**, 8169-8172 (2014).

14 Lerch, M. M., Szymański, W. & Feringa, B. L. The (photo) chemistry of Stenhouse photoswitches: guiding principles and system design. *Chem. Soc. Rev.* **47**, 1910-1937 (2018).

15 Hemmer, J. R. *et al.* Tunable visible and near infrared photoswitches. *J. Am. Chem. Soc.* **138**, 13960-13966 (2016).

16 Mallo, N. *et al.* Photochromic switching behaviour of donor-acceptor Stenhouse adducts in organic solvents. *Chem. Commun.* **52**, 13576-13579 (2016).

17 Duan, Y. *et al.* Controlling the isomerization of photoresponsive molecules through a limiting tautomerization strategy. *J. Phys. Chem. B* **126**, 3347-3354 (2022).

18 Hemmer, J. R. *et al.* Controlling dark equilibria and enhancing donor-acceptor Stenhouse adduct photoswitching properties through carbon acid design. *J. Am. Chem. Soc.* **140**, 10425-10429 (2018).

19 Overholts, A. C., Granados Razo, W. & Robb, M. J. Mechanically gated formation of donor-acceptor Stenhouse adducts enabling mechanochemical multicolour soft lithography. *Nat. Chem.* **15**, 332-338 (2023).

20 Sun, F. *et al.* Fast photochromism in solid: microenvironment in metal-organic frameworks promotes the isomerization of donor-acceptor stenhouse adducts. *Chem. Eng. J.* **427**, 132037 (2022).

21 Sroda, M. M., Stricker, F., Peterson, J. A., Bernal, A. & Read de Alaniz, J. Donor-acceptor Stenhouse adducts: exploring the effects of ionic character. *Chem. Eur. J.* **27**, 4183-4190 (2021).

22 Schreiber, B., Martinek, H., Wolschann, P. & Schuster, P. Kinetic studies on the nucleophilic addition to double bonds. 1. Addition of amines to electrophilic carbon-carbon double bonds. *J. Am. Chem. Soc.* **101**, 4708-4713 (1979).

23 Stricker, F. *et al.* A multi-stage single photochrome system for controlled photoswitching responses. *Nat. Chem.* **14**, 942-948 (2022).

24 Mallo, N. *et al.* Structure-function relationships of donor-acceptor Stenhouse adduct photochromic switches. *Chem. Sci.* **9**, 8242-8252 (2018).

25 Rifaie-Graham, O. *et al.* Photoswitchable gating of non-equilibrium enzymatic feedback in chemically communicating polymersome nanoreactors. *Nat. Chem.* **15**, 110-118 (2023).

26 Stricker, F. et al. Selective control of donor-acceptor Stenhouse adduct populations with non-selective stimuli. Chem (2023).

27 Swinehart, D. F. The beer-lambert law. *J. Chem. Educ.* **39**, 333 (1962).

28 Jeffery, G. *Quantitative chemical analysis*. (New York, 1989).

29 Schanda, J. *Colorimetry: understanding the CIE system*. (John Wiley & Sons, 2007).

30 Ohta, N. & Robertson, A. *Colorimetry: fundamentals and applications*. (John Wiley & Sons, 2006).

31 Alves, J., Wiedbrauk, S., Barner-Kowollik, C. & Blinco, J. P. The missing piece: concentration dependence of donor-acceptor Stenhouse adduct (DASA) reactivity. *ChemPhotoChem* **5**, 711-715 (2021).

32 Lui, B. F. *et al.* Unusual concentration dependence of the photoisomerization reaction in donor-acceptor Stenhouse adducts. *Photochem. Photobiol. Sci.* **18**, 1587-1595 (2019).

33 Berns, R. S. *Billmeyer and Saltzman's principles of color technology*. (John Wiley & Sons, 2019).

34 Robertson, A. R. Historical development of CIE recommended color difference equations. *Color Res. Appl.* **15**, 167-170 (1990).

35 Sharma, G. & Bala, R. *Digital color imaging handbook*. (CRC press, 2017).

36 Sun, F. & Wang, D. Toward real-world applications: promoting fast and efficient photoswitching in the solid state. *J. Mater. Chem. C* **10**, 13700-13716 (2022).

37 Xiong, X. *et al.* Ester matters? Promoting photoisomerization of donor-acceptor Stenhouse adducts in the solid state and "burn after reading" encryption. *Chem. Eng. J.* **450**, 138090 (2022).

## Data availability

The data that support the findings of this study are available from the corresponding author upon reasonable request.


## Acknowledgments

We thank Y. Liu, C. S. Zhao, L. Q. Chen, H. Zhao, C. M. Xie, Q. Wei, B. He, X. D. Liu, L. J. Mao for their kind discussions. This work was supported by the National Natural Science Foundation of China (52203134).


## Author contributions

F. S. and D. W. conceived the research, designed the experiments and wrote the manuscript. D. W. C. W.and Y. Z. supervised the research. F. S., A. G., H. Z. and D. D. carried out the experiments. B. Y. and J. Z. built the analytical models. X. D., C. W. and X. W. jointly supervised this work. Y. Z and D. W. supervised this work. All authors analysed and interpreted the data and wrote the paper.


## *Corresponding authors*

Correspondence to Y. Zheng, C. Wei and D. Wang.


## Ethics declarations

## Competing interests

The authors declare no competing interests.

## Additional information

## Supplementary information

### *Supplementary information*

The supplementary information includes materials and characterization, crystal structure supplementary code, supplementary methods, supplementary discussion, supplementary figures, supplementary table and supplementary references.

***Supplementary Video 1: Active camouflage of SAP solutions in black, red, green, and yellow acrylic boxes.***

The left cuvette was loaded with SAP solutions and the right cuvette with black ink as the control. Black dots represent the in situ distance between the average RGB values of regions C and B, and colored dots represent the distance between regions A and B. The video was speeded up and the timing information of the original video was embedded in the video.

***Supplementary Video 2: Color switching of SAP solutions below black, red, orange, yellow and green acrylic plates.***

The SAP solutions were placed below black, red, orange, yellow and green arylic plates. The video was speeded up and the timing information of the original video was embedded in the video.

***Supplementary Video 3: Color switching of SAP solutions in red, green and yellow bushes.***

The SAP solutions were placed in red (*Cyclamen persicum*), green (*Epipremnum aureum*) and yellow (*Ginkgo*) bushes, and a white light LED was set to the left of the plants. The video was speeded up and the timing information of the original video was embedded in the video.

***Supplementary Video 4: Color switching of SAP solutions below red petal, green leaf and yellow leaf.***

SAP solutions were placed below red petal, green leaf and yellow leaf. The video was speeded up and the timing information of the original video was embedded in the video.

***Supplementary Video 5: Color switching of SAP solutions under red, orange, yellow and green umbrellas.***

SAP solutions were set under red, orange, yellow and green umbrellas, respectively, which were put under sunlight (60000 lux, 37 °C, and bottles were stored in the dark and immersed in liquid nitrogen for 5 s before the experiments). The video was speeded up and the timing information of the original video was embedded in the video.

***Supplementary Video 6: Active camouflage of SAP solutions under red, orange, yellow and green umbrellas.***

SAP solutions were set under a red umbrella, which were put under sunlight (60000 lux, 37 °C, and bottles were stored in the dark and immersed in liquid nitrogen for 5 s before the experiments). The umbrella was changed by yellow and green umbrellas sequentially. The video was speeded up and the timing information of the original video was embedded in the video.

***Supplementary Video 7: Active camouflage of SAP solutions in NMR tube below sequentially arranged sticky notes.***

SAP solution was filled into a NMR tube, which was covered with sequentially arranged red, green and yellow sticky notes. A white light LED was set on the top. The video was speeded up and the timing information of the original video was embedded in the video.

***Supplementary Video 8: Color switching of SAP films upon light irradiation with corresponding wavelength.***

SAP films were irradiated by 660, 520 and 590 nm light irradiation, respectively. The video was speeded up and the timing information of the original video was embedded in the video.

***Supplementary Video 9: Color switching of ABS models upon light irradiation with corresponding wavelength.***

ABS models coated with SAP coatings were irradiated by 660, 520 and 590 nm light irradiation, respectively. The video was speeded up and the timing information of the original video was embedded in the video.

## Methods

### Synthesis

The synthesis of the color-contributing units was shown in **Extended data Fig. 1**.

*Synthesis of F1.* 2,2-dimethyl-1,3-dioxane-4,6-dione (1.44 g, 10 mmol) was dissolved into 30 mL distilled water under stirring. After slowly dropping 2-furaldehyde (0.96 g, 10 mmol), the solution was heated to 40 ºC and kept for 2 h. The formed yellow solid was collected by vacuum filtration, followed by washing with distilled water. The solid was dissolved into 30 mL DCM and sequentially washed with 30 mL saturated $NaHSO_3$ aqueous solution and 30 mL saturated NaCl aqueous solution for 2 times. The organic layer was dried with $Na_2SO_4$ and purified by column chromatography, obtaining 2.11 g yellow product (Yield: 95%)[13]. The single crystal structure of F1 is shown in **Supplementary Fig. 2**.

*Synthesis of F3.* 1,3-dimethylbarbituric acid (1.56 g, 10 mmol) and 4-(dimethylamino)benzaldehyde (1.49 g, 10 mmol) were dissolved into 25 mL ethanol. The solution was then heated to 90 ºC under vigorous sitting for 4 h. The red precipitates were collected by filtration and dried overnight to obtain 2.59 g red solid (Yield: 90%)[22]. The single crystal structure of F3 is shown in **Supplementary Fig. 3**.

*Synthesis of F4.* 1-phenyl-3-(trifluoromethyl)-1H-pyrazol-5(4H)-one (2.28 g, 10 mmol) and 4-(dimethylamino)benzaldehyde (1.49 g, 10 mmol) were dissolved into 25 mL ethanol. The solution was then heated to 90 ºC under vigorous sitting for 4 h. The red precipitates were collected by filtration and dried overnight to obtain 3.23 g brown solid (Yield: 90%). The single crystal structure of F4 is shown in **Supplementary Fig. 4**.

*Synthesis of D1.* F1 (1.11 g, 5 mmol) was dissolved into 50 mL DCM, followed by slowly adding n-propylaniline (0.68 g, 5 mmol). The reaction was kept stirring at 40 ºC and monitored by thin

layer chromatography (TLC). The mixture was condensed by rotary evaporation and further purified by column chromatography to give 0.89 g D1 as deep purple solid (Yield: 50%)[20]. The single crystal structure of D1 is shown in **Supplementary Fig. 5**.

*Synthesis of D2.* F1 (1.11 g, 5 mmol) was dissolved into 50 mL DCM, followed by slowly adding indoline (0.60 g, 5 mmol). After stirring at 40 ºC for 2 h, the solution was condensed by rotary evaporation and redissolved in the minimum amount of DCM in a 250 mL beaker. 100 mL cold hexane (-20 ºC) was slowly poured into the beaker, which was then transferred to a refrigerator at -20 ºC for 30 min and slowly stirred for 5 min. The purple solid was filtered and further purified by column chromatography to give 1.02 g D2 (Yield: 60%)[15]. The single crystal structure of D2 is shown in **Supplementary Fig. 6**.

*Synthesis of D3.* 1,3-dimethylbarbituric acid (1.56 g, 10 mmol) was dissolved into 30 mL distilled water under stirring. After slowly dropping 2-furaldehyde (0.96 g, 10 mmol), the solution was heated to 40 ºC and kept for 2 h. The formed yellow solid was collected by vacuum filtration, followed by washing with distilled water. The solid was dissolved into 30 mL DCM and sequentially washed with 30 mL saturated $NaHSO_3$ aqueous solution and 30 mL saturated NaCl aqueous solution for 2 times. The organic layer was dried with $Na_2SO_4$ and purified by column chromatography, obtaining 1.99 g yellow product as the intermediate (Yield: 85%).

The intermediate (1.17 g, 5 mmol) was dissolved into 50 mL DCM, followed by slowly adding indoline (0.60 g, 5 mmol). After stirring at 40 ºC for 2 h, the solution was condensed by rotary evaporation and redissolved in the minimum amount of DCM in a 250 mL beaker. 100 mL cold hexane (-20 ºC) was slowly poured into the beaker, which was then transferred to a refrigerator at -20 ºC for 30 min and slowly stirred for 5 min. The dark blue solid was filtered and

523 further purified by column chromatography to give 0.88 g D3 (Yield: 50%)[15]. The single crystal
524 structure of D3 is shown in **Supplementary Fig. 7**.

525 *Synthesis of D4.* 1-phenyl-3-(trifluoromethyl)-1H-pyrazol-5(4H)-one (2.28 g, 10 mmol) and 2-
526 furaldehyde (0.96 g, 10 mmol) were dissolved into 30 mL DCM and stirred for 2 h at 40 °C. The
527 mixture was condensed by rotary evaporation, which was washed with water and further purified
528 by column chromatography to give 2.45 g intermediate as dark red solid (Yield: 80%).

529 The intermediate (1.53 g, 5 mmol) was dissolved into methanol at 20 °C, followed by slowly
530 adding Indoline (0.60 g, 5 mmol). Green crystal-like solid slowly precipitated from the dark blue
531 solution, which was filtered and washed serval times with cold methanol. The solid was collected
532 and dried overnight to give 1.47 g D4 (Yield: 70%)[21]. The single crystal structure of D4 is shown
533 in **Supplementary Fig. 8**.

534 **Photoisomerization of DASAs**

535 *Preparation of DASAs solutions.* PCL was dissolved into the mixed solvent of DCM and THF (9:1,
536 v/v) with the concentration of 0.1 g/mL under stirring. DASAs were dissolved into the mixture
537 with a specific concentration to make the initial absorbance between 0.5 and 1.5, ensuring the
538 accuracy of the spectrophotometer, which was sealed and stored at room temperature in the dark.

539 *Experimental setup.* LED lights with the emission wavelength at 520 nm (green), 590 nm (yellow),
540 620 nm (orange), and 660 nm (red) were used to induce the *linear*-to-*cyclic* isomerization of
541 DASAs (D1-D4). The interrelationship between the intensity of irradiation and distance was
542 monitored with an illuminometer (**Extended Data Fig. 2a**). The distance between the sample and
543 LEDs were set as 5 cm, 10 cm, 30 cm, 50 cm, 75 cm, 100 cm, and 200 cm (**Extended Data Fig.**
544 **3a**). The temperature was maintained at 25 °C. Each kinetic measurement lasts 1800 s.

*Data processing.* DASAs in *cyclic* do not absorb in the visible light region[14], therefore, the *linear*-to-*cyclic* isomerization induces the decrease in absorbance. Based on the Lambert-Beer law, the absorbance is linearly dependent with the concentration[27]. Therefore, the portion of *linear* DASAs at any given time ($L_t$) was obtained by the following equation.

$$L_t = \frac{A_t - A_{baseline}}{A_{0\,s} - A_{baseline}} \times 100\% \quad (3)$$

The *linear* DASAs content (%) at equilibrium($L_e$) is obtained by fitting[15,24] (equation 1) except in three scenarios 1) when the R-square is lower than 90%; 2) when the fitted *linear*% is negative (slightly lower than zero); 3) when the first-order exponential function is not applicable to describe *linear*-to-*cyclic* isomerization, for example, while using an irrelevant light to irradiate the DASAs that has no or little absorption in corresponding wavelength at low intensity (irradiating D1 with 660 nm at 200 cm), no or little isomerization occurs. For these invalid fitting data, the *linear*% at equilibrium($L_{e'}$) is obtained by only considering the starting($L_{0\,s}$) and ending($L_{1800\,s}$) *linear*%, by following equation.

$$L_{e'} = \frac{L_{1800\,s}}{L_{0\,s}} \times 100\% \quad (4)$$

The raw data of absorbance and transformed *linear* content at each time interval are shown in **Supplementary Table 4-32**.

## Optimizing the SAP materials

*Obtain the L*, a*, b* values.* The simulated transmission spectra of SAP solutions were input into the plugin of OriginLab (Chromaticity Diagram, Transmittance (0-1), mode D65, Standard Observer CIE 1931 2°) to obtain the $L^*$, $a^*$, $b^*$ values[30]. To make a direct investigation on the color, the $a^*$ $b^*$ coordinates were constructed in the chromaticity diagram. For the selection of

color-contributing units, the $L^*$, $a^*$, $b^*$ values of the SAP solutions of A2, A4, A6, R6, A8, and R8 were calculated (**Supplementary Table 34**). Besides, A4 solutions with the initial absorbance between 0.5 and 50 were investigated (**Supplementary Table 35**). For the investigation of the SAP solutions under light irradiation, the cumulative absorption spectra were calculated via the equilibrated *linear* content (%) of D1 and D4, the data were obtained from **Fig.1e**, **Extended Data Fig. 3b** and **Supplementary Table 32**. The absorption and transmission spectra of the SAP solutions were recorded in **Supplementary Fig. 12-20**, which were further transferred into the $L^*$, $a^*$, $b^*$ values and recorded in the chromaticity diagram (**Supplementary Table 36-44** and **Extended Data Fig. 4d** and **4f**).

*Determine the accuracy of color.* The accuracy of color without light irradiation (black state) was determined by the sum of $L^*$ and SQRT($a^{*2}$+$b^{*2}$), which represent lightness and deviation, respectively[29]. The SQRT($a^{*2}$+$b^{*2}$) was obtained through the following equation.

$$SQRT(a^{*2} + b^{*2}) = \sqrt{a^{*2} + b^{*2}} \tag{5}$$

The absorption spectra of A4 under light irradiation with different wavelengths and intensities were calculated by accumulating the spectra of color-contributed units at photostationary state through the following equation[27].

$$A = a\varepsilon_{F1} + c\varepsilon_{F3} + e[L_{eD1}\varepsilon_{lD1} + (1 - L_{eD1})\varepsilon_{cD1}] + h[L_{eD4}\varepsilon_{lD4} + (1 - L_{eD4})\varepsilon_{cD4}] \tag{6}$$

$L_{eD1}$ and $L_{eD4}$ represent the *linear* content at equilibrium for D1 and D4; $\varepsilon_{lD1}$, $\varepsilon_{cD1}$, $\varepsilon_{lD4}$ and $\varepsilon_{cD4}$ represent the molar absorption coefficients for *linear* D1, *cyclic* D1, *linear* D4 and *cyclic* D4, respectively. Theoretically, the $\varepsilon_{cD1}$ and $\varepsilon_{cD4}$ are equal to 0 between the wavelengths of 400 and 700 nm, due to the dispersed conjugation of *cyclic* DASAs. The information of calculated absorbance spectra was shown in **Supplementary Fig.12-20**.

In the chromaticity diagram, the color of SAP solutions after light irradiation is recorded with a dot with specific $a^*b^*$ values, while the color of light is recorded with a straight line across the origin of coordinate[29]. The direction of the line is determined according to the emission spectra of the LEDs(**Extended data Fig. 2b**). The accuracy of color under light irradiation (colored state) was determined by the difference of angle ($\Delta\theta$) in the chromaticity diagram between the SAP solutions (dot, $\theta_D$) and corresponding light (line, $\theta_L$). For any dot with a specific $a^*b^*$ value, the $\theta_D$ could be calculated by the following equation.

$$\theta(a^*, b^*) = \begin{cases} arctan(b^*/a^*), & b^*/a^* > 0 \\ arctan(b^*/a^*) + 180, & b^*/a^* < 0 \end{cases} \quad (7)$$

Sequentially, the $\Delta\theta$ could be obtained by the following equation, and the results were recorded in **Supplementary Table 47-55**.

$$\Delta\theta = \theta_D - \theta_L \quad (8)$$

**Active camouflage of SAP solutions**

*Preparation of SAP solutions.* The color-contributing units were dissolved into the mixture of PCL, DCM and THF to prepare SAP solutions. A4 with the initial absorbance of 6 was selected for the fabrication. F1, F3, D1 and D4 were dissolved into the mixed solvent, while the absorbance at 362 , 461 , 556 and 645 nm were kept at 3 (in a 0.5 cm cuvette). Due to the spontaneously occurred *linear*-to-*cyclic* isomerization of D1, the absorbance at 556 nm decreases sharply at the end of the first day[15,24] (**Supplementary Fig. 21a-b**). The absorbance at 556 nm keeps decreasing the in the second and third day, which however is less than the first day. Therefore, we used a "little and often" strategy to prepare the SAP solutions. After the first day, a small amount of D1 was added to make the absorbance at 556 nm reaches 3 again (**Supplementary Fig. 21c-d**). This step was

repeated at the third day. The absorbance does not obviously change after 3 days (**Supplementary Fig. 21e-f**). The SAP solutions were sealed and stored in the dark under room temperature.

*Processing of the video for active camouflage.* The video of active camouflage with acrylic boxes was processed to quantitatively determine the camouflage property of SAP solutions. The LAB color space is based on the human eye's perception of colors and represent all the colors those the human eyes can perceive.[29] "L" represents the lightness, "A" represents the red-green color difference, and "B" represents the blue-yellow color difference. The total color difference (ΔE) between the two colors is calculated as the following equation[35].

$$\Delta E = \sqrt{\Delta L^2 + \Delta A^2 + \Delta B^2} \tag{9}$$

To make the calculation simpler, we used a weighted Euclidean distance formula in RGB color space to determine the color difference, as shown in equations S7-S9[34].

$$\overline{r} = \frac{C_{1,R} + C_{2,R}}{2} \tag{10}$$

$$\begin{cases} \Delta R = C_{1,R} - C_{2,R} \\ \Delta G = C_{1,G} - C_{2,G} \\ \Delta B = C_{1,B} - C_{2,B} \end{cases} \tag{11}$$

$$\Delta C = \sqrt{\left(2 + \frac{\overline{r}}{256}\right) \times \Delta R^2 + 4 \times \Delta G^2 + \left(2 + \frac{255 - \overline{r}}{256}\right) \times \Delta B^2} \tag{12}$$

In this formula, $\overline{r}$ is the average value of the red channel of colors $C_{1,R}$ and $C_{2,R}$ ($C_1$ and $C_2$ represent any two channels in the video for comparison), $\Delta R$ is the difference between the red channel values of colors $C_{1,R}$ and $C_{2,R}$, $\Delta G$ is the difference between the red channel values of colors $C_{1,R}$ and $C_{2,R}$, $\Delta B$ is the difference between the red channel values of colors $C_{1,R}$ and $C_{2,R}$.

To eliminate the side effects in the video such as reflection on the cuvette, rectangular regions with the size of 10*40 pixels were selected on both the samples (SAP solution and black ink) and on the acrylic box (as the background), respectively (**Fig. 3d**). For each frame of the video, the average values of the R, G, and B channels within the selected rectangular region were calculated. The color difference on the SAP solution (A), background (B), and black ink (C) were calculated. The source code for the processing of video is available.

## SAP in the solid state

*Fabrication of SAP films.* The SAP film was fabricated by spin-coating with the rotate speed of 500 rpm, rotational acceleration of 100 rpm/s and spin coating time of 60 s. Glass was used as the substrate. After spin-coating, the substrate was annealed in the vaccum oven at 80 ºC for 30 min, obtaining a relatively flat and smooth surface. The film was carefully peeled off from the glass substrate.

*Coating on figurine models.* The SAP coatings were prepared in a similar procedure with that for the SAP solutions. The SAP coatings were spray-coated onto the surface of figurine models made of ABS. A commercial spray-coating suit was used, the nozzle diameter is 0.5 mm, the distance between the tube and model is kept at 3 cm, the air pressure is set between 15-30 psi. During the spray-coating, the moving speed of the spraying gun is controlled at 5 cm/s. The spray-coating is repeated for 10 times to make the film thick enough (**Supplementary Fig. 22**). After coating, the substrates were annealed by a temperature-adjustable heat gun at 150 ºC for 10 s, which generates a smooth surface (**Supplementary Fig. 23**).

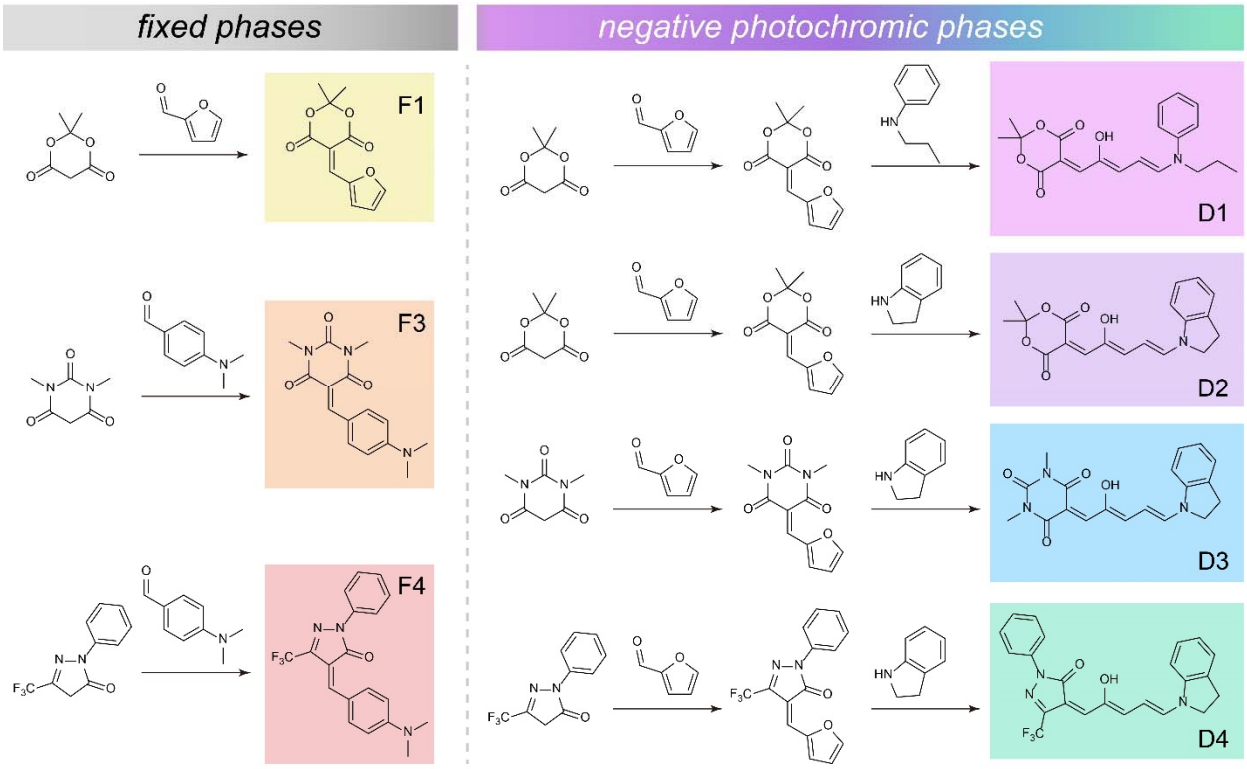


**Extended Data Fig. 1 | Synthesis of the color-contributing units.** Synthetic route for F1, F3, and F4 as fixed phases, and D1, D2, D3, and D4 as negative photochromic phases.

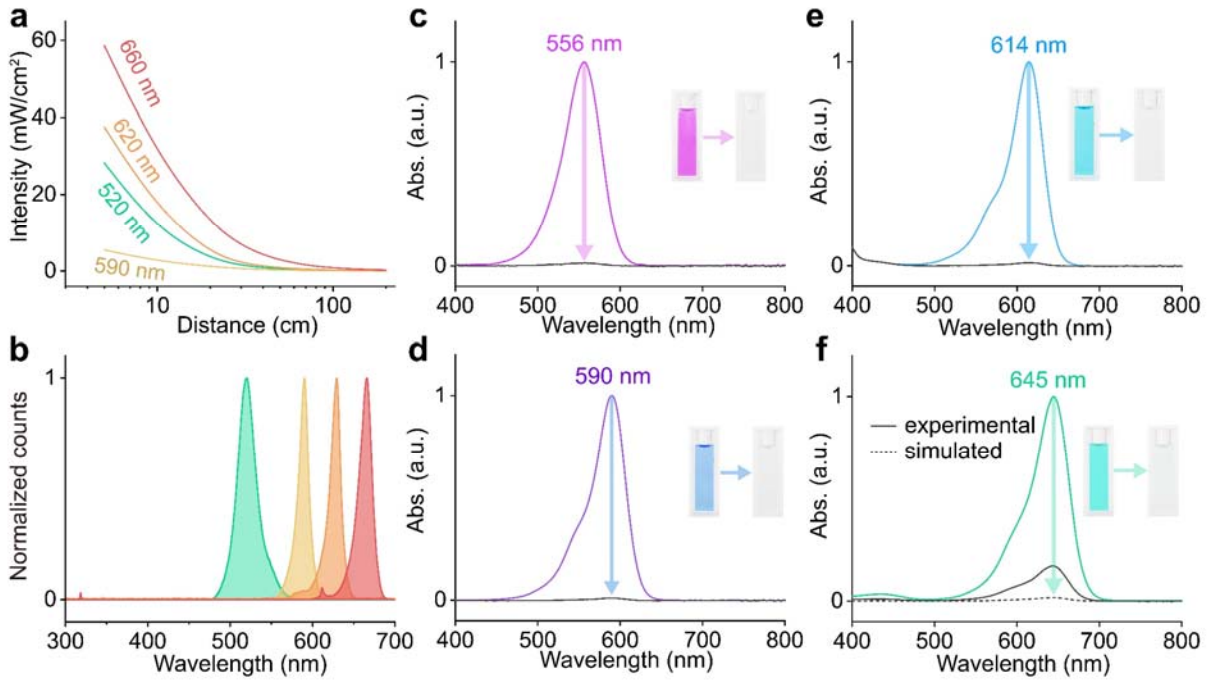


**Extended Data Fig. 2 | Synthesis of the color-contributing units. a,** Relationships between light intensity and distance. **b**, Normalized luminescence spectra of LED light sources of 520 nm, 590 nm, 620 nm, and 660 nm. **c-f** UV-vis absorption spectra of D1, D2, D3, and D4 before and after visible light irradiation (inner shows the photographic images of the photochromism).

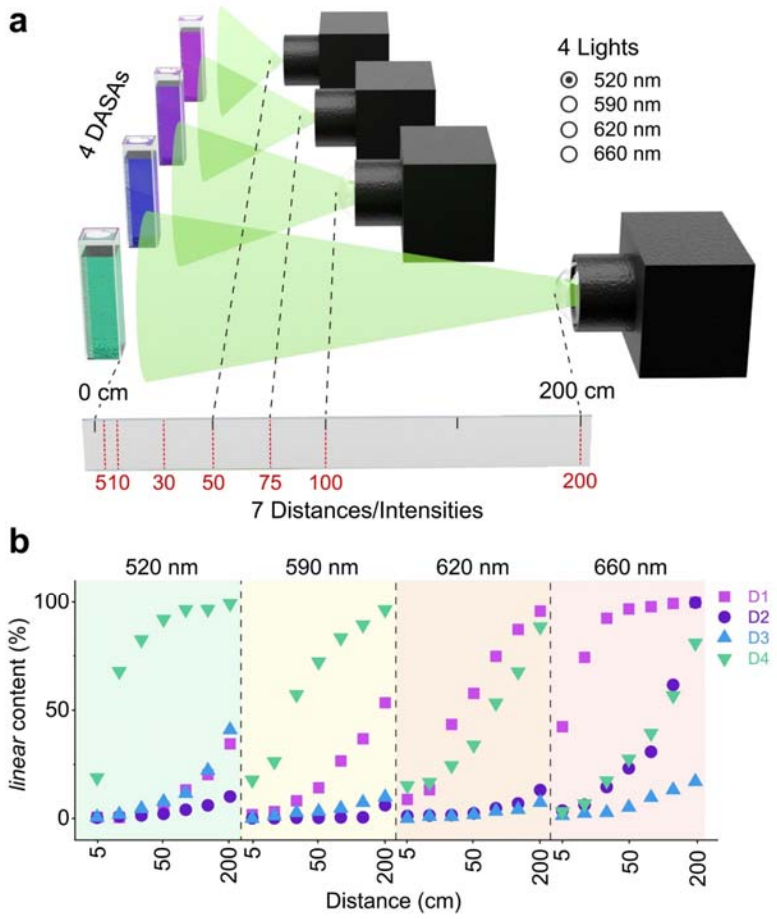


673

674 **Extended Data Fig. 3 | Equilibrium of DASAs under light irradiation. a,** Schematic illustration of the
675 experimental setup for testing the dynamics of isomerization of DASAs under light irradiation with
676 different wavelengths and intensities. The intensity was varied by controlling the distance between the
677 samples and LEDs. **b,** *linear* content (%) of DASAs at equilibrium under 520 nm, 590 nm, 620 nm, and
678 660 nm light irradiation. The distance between the sample and the LEDs was kept between 5 cm and 200
679 cm.

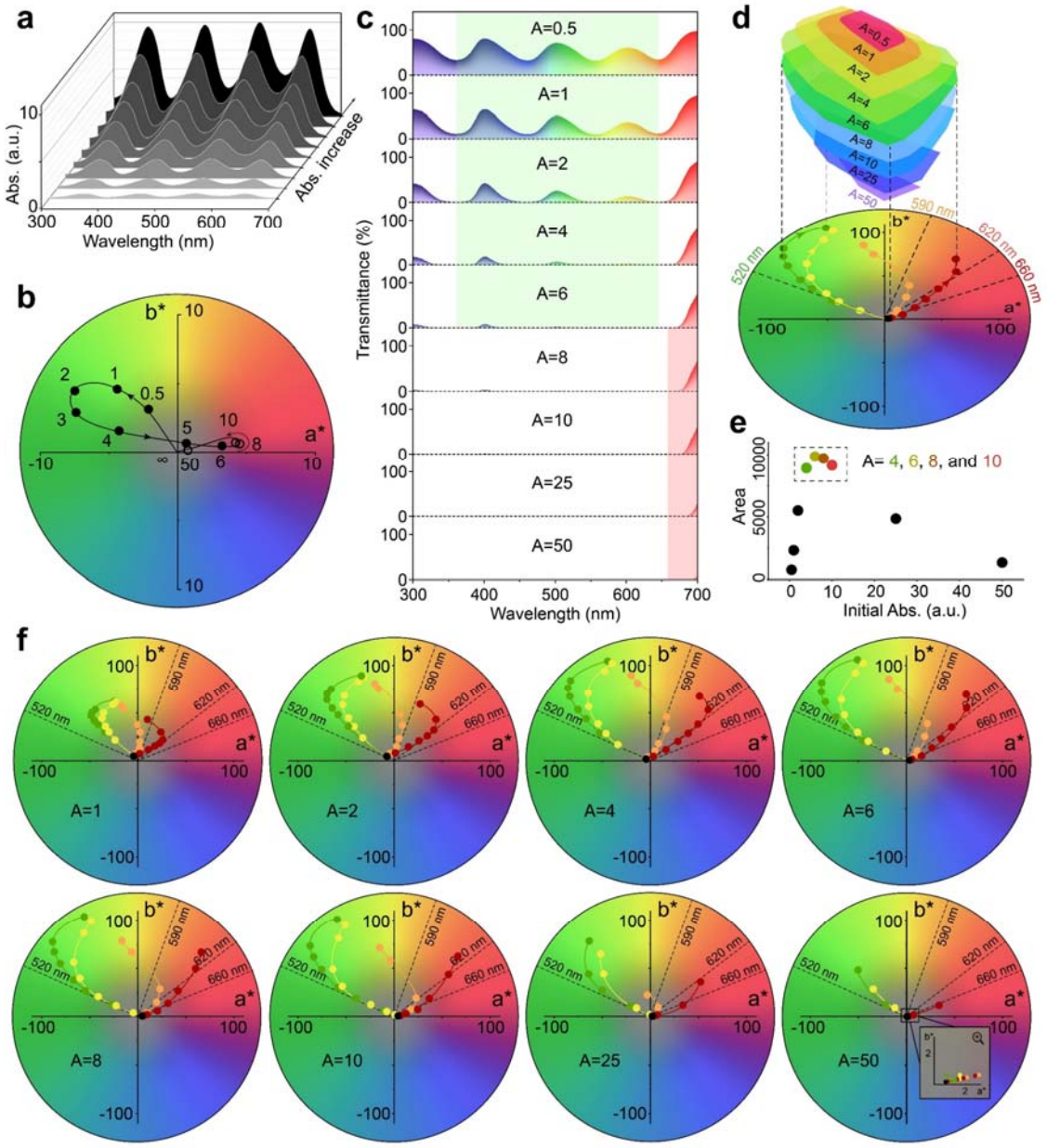


**Extended Data Fig. 4 | The accuracy of color for the A4 solutions. a**, Simulated UV-vis absorption spectra of A4 solutions with the initial absorbance increasing from 0.5 to 10 (A=25 and 50 are not shown). **b**, Modified CIE 1931 a* b* values of A4 solutions with the initial absorbance increasing from 0.5 to 50. **c**, Simulated UV-vis transmission spectra of A4 solutions with various initial absorbance. **d**, Top half: Tunable range of color for A4 solutions with various initial absorbance; Down half: Modified CIE 1931 a* b* values of A4 solutions (A=6) under 520 nm (green), 590 nm (yellow), 620 nm (orange), and 660 nm (red) light irradiation, the distance was kept at 5 cm, 10 cm, 30 cm, 50 cm, 75 cm, 100 cm, and 200 cm, dash lines stand for the color of LED lights. **e**, Summarized tunable range of color for A4 solutions. **f**, Modified CIE 1931 *a*b** values of A4 solutions (Abs=0.5, 1, 2, 4, 8, 10, 25, and 50) under 520 nm (green), 590 nm (yellow), 620 nm (orange), and 660 nm (red) light irradiation, the distance was kept at 5 cm, 10 cm, 30 cm, 50 cm, 75 cm, 100 cm, 200 cm, dash lines stand for the color of LED lights.

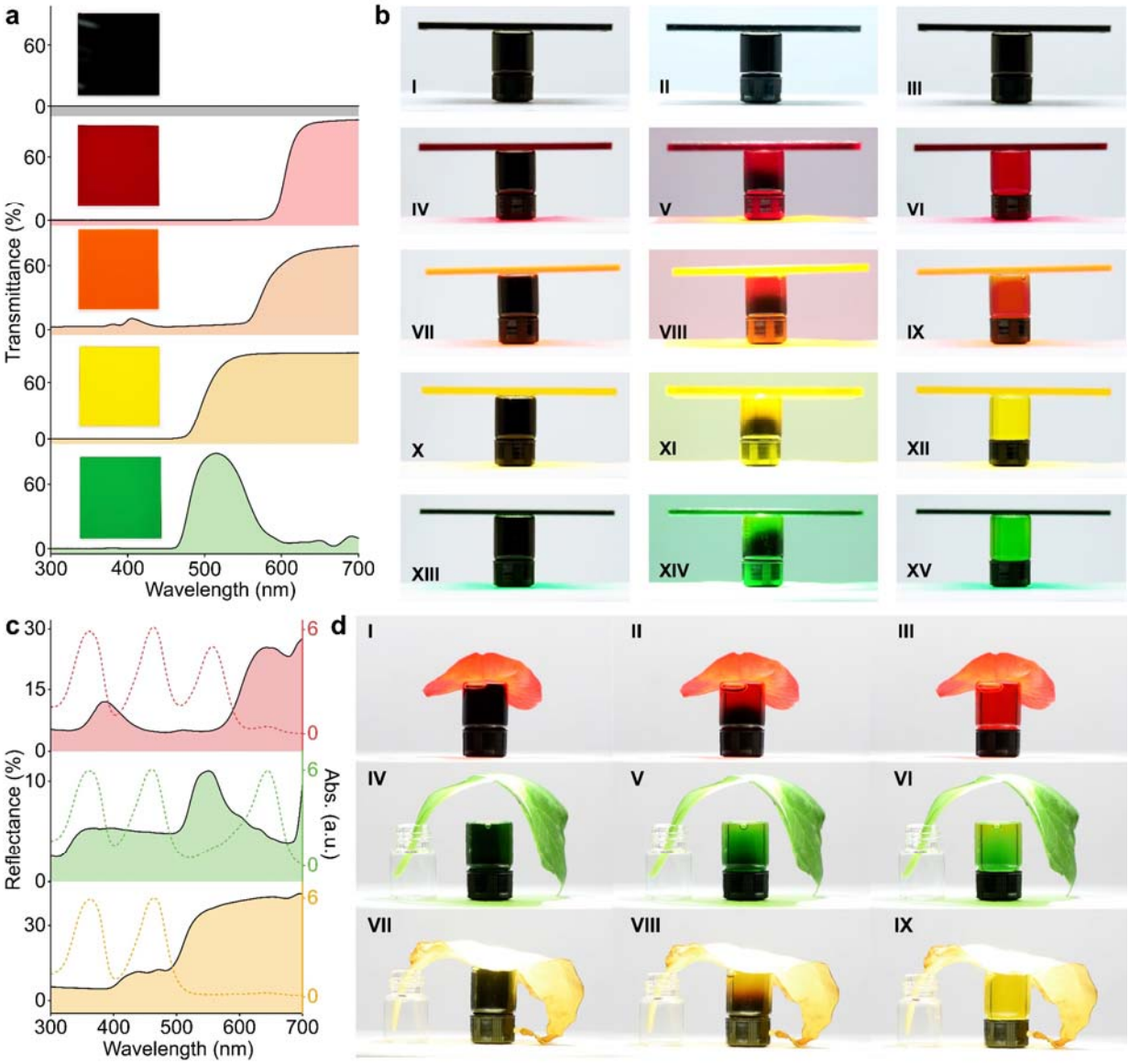


692

693 **Extended Data Fig. 5 | Self-adaptive color-changing process of SAP solutions. a,** Transmission spectra
694 and images of red, orange, yellow and green acrylic plates. **b,** Video screenshots of the self-adaptive color-
695 changing process of SAP solutions under red, orange, yellow and green acrylic plates. **c,** UV-vis diffuse
696 reflectance spectra of *Cyclamen persicum* (red), *Epipremnum aureum* (green), and *Ginkgo* (yellow) and the
697 UV-vis absorption spectra of the corresponding SAP solutions. **d**, Video screenshots of the self-adaptive
698 color-changing process of SAP solutions under red petal, green leaf and yellow leaf.

699

700

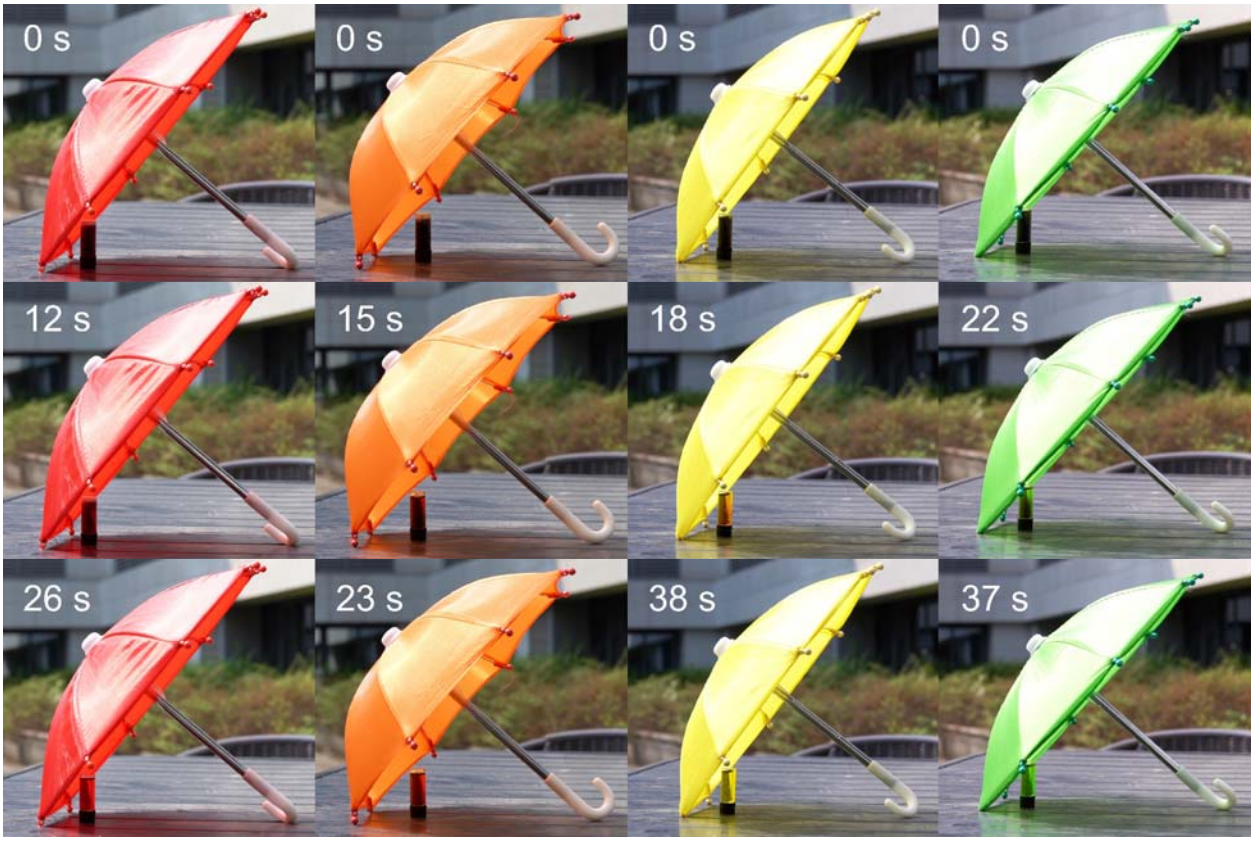


**Extended Data Fig. 6 | SAP in practical. a,** Photographic images of hiding SAP solutions into red, orange, yellow and green umbrellas under sunlight.

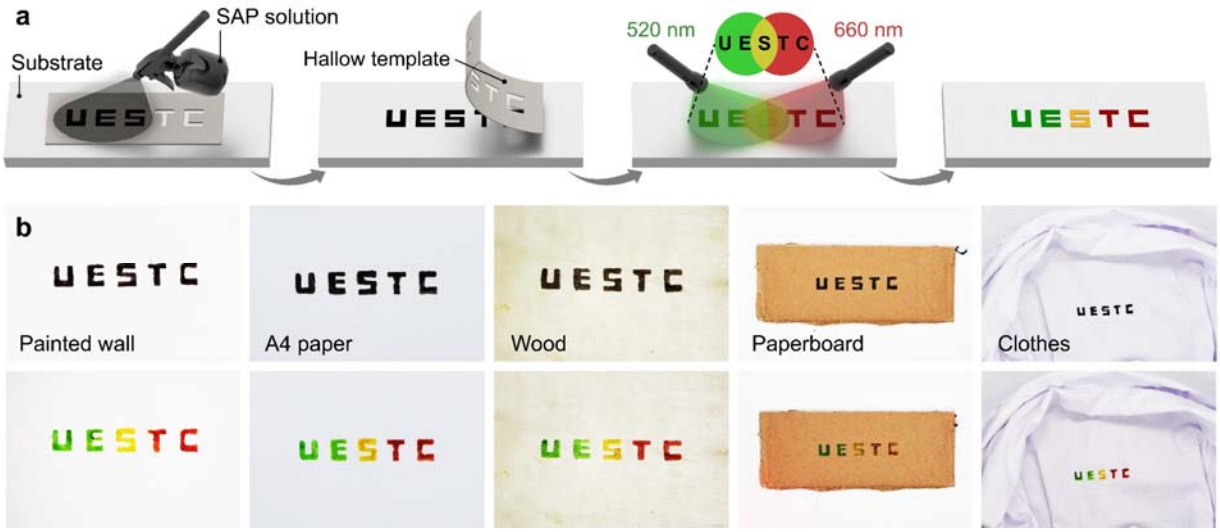


**Extended Data Fig. 7 | SAP in the solid state. a,** Schematic illustration of the mask-assisted spray-coating process and irradiation method of green light (520 nm), red light (660 nm) and mixed yellow light. **b,** Images of SAP coating on rough surfaces (painted wall, A4 paper, wood, paperboard and clothes), images of the above surfaces irradiated by green light(520 nm), red light(660 nm) and mixed yellow light.